Int J Adv Manuf Technol (2015) 79:541–550
DOI 10.1007/s00170-015-6816-9

ORIGINAL ARTICLE

Research on the cutting mechanism of cylindrical gear power skiving

Erkuo Guo · Rongjing Hong · Xiaodiao Huang · Chenggang Fang

Received: 9 October 2014 / Accepted: 18 January 2015 / Published online: 10 February 2015

Abstract Latest research clearly demonstrates the excellent capability of the gear power skiving technology. For further improvement of the skiving process and enhancement of the process reliability, the fundamental research on the cutting mechanism of cylindrical gear power skiving was conducted. First, the kinematic model of power skiving and mathematical of tapered skiving cutter were established according to the engagement principle of crossed helical gears. Then, the simulation process and chip deformation mechanism were developed. Based on the proposed modeling, we investigated the cutting mechanism, including the cutter top rake angle related to the cut strategy, skiving accuracy with respect to the gear number, and tooth ratio. The results support the skiving cutter design and process optimization and are an important basis for the implementation of the advanced gear process.

Keywords Cylindrical gears · Power skiving · Tapered skiving cutter · Cutting mechanism

Abbreviations

Σ	Setting angle of the cutter
β_1	Helix angle of workpiece
β_2	Helix angle of cutter
$\boldsymbol{v}$	Cutting velocity
$\boldsymbol{v}_1$	Speed of skiving cutter
$\boldsymbol{v}_2$	Speed of workpiece
$\boldsymbol{v}_{1a}$	Axial speed of skiving cutter
$\boldsymbol{v}_{1t}$	Tangential speed of skiving cutter
$\boldsymbol{v}_t$	Resultant speed of workpiece
$\boldsymbol{v}_0^{(2)}$	Axial feed of workpiece
ω_1	Angular velocity of skiving cutter
ω_2	Angular velocity of workpiece
$\Delta\omega_1$	Incremental angular velocity of ω_1
m_n	Normal module of tooth
β_1	Helix angle of skiving cutter
β_2	Helix angle of gear
Z_t	Teeth number of cutter
Z_g	Teeth number of gear
i_{21}	Ratio between cutter and gear
a	Center distance between the cutter and workpiece
l_2	Axial incremental movement
φ_1, φ_2	Rotation angles of skiving cutter and workpiece
n_1, n_2	Rotation speeds of skiving cutter and workpiece
(u, θ)	Surface parameters
P	Screw parameter
r_b	Radius of base circle
σ_0	Half angular tooth thickness on the base circle
b	Width of gear
p	Screw parameter of helical gear
f_z	Axial feed per gear rotation
α_p	Radial feed of cutter
h_D	Nominal maximum chip thickness
γ_z	Top rake angle
α_z	Top relief angle
λ_z	Side relief angle
F_β	Lead deviation of gear

1 Introduction

It has been known that the power skiving process for machining internal gears is multiple times faster than shaping, and more flexible than broaching, due to skiving's continuous chip

E. Guo · R. Hong (✉) · X. Huang · C. Fang
College of Mechanical and Power Engineering, Nanjing Tech University, Nanjing 211800, China
e-mail: hongjmst@sina.com

removal capability. The patent of the skiving process was assigned in the beginning of the 20th century. However, the method was not implemented at that time because power skiving has always presented a challenge to machines and skiving cutters. M. Kojima [1, 2] has studied the productive method in 1974; the geometrical relationships between skiving cutter and spur gears were analyzed according to the analytical theory of tooth profile, and the clearance angles of skiving cutter were investigated numerically. With the improvements in numerical control of direct drive train, stiff electronic gearboxes, complex tool geometry, and the fast coating technology, latest research demonstrates that power skiving is capable of being a high-productive and flexible alternative to the advanced technology in market [3, 4].

The current developments were initiated at the Institute of Production Science with a numerical method to calculate the tools [5]; the power skiving was considered as a contemporary gear pro-machining solution and the economic and environment friendly aspect of the power skiving process were explained. The subsequent methodical experimental analyses indicated the potential and advantages as mentioned above [6, 7]. Volker [8] established a 3D-FEM model of gear skiving to investigate the kinematical conditions as well as chip formation mechanisms and evaluation of the effects on process reliability. Hartmut and Olaf [9] proposed a semi-completing skiving method and apparatus for gear power skiving, then [10] they provided a new method to improve the uniformity of load to both flank cutting edges and extend the longest possible tool service life. Li and Chen [11, 12] proposed a slicing technology for cylindrical gears to improve the limitation of current gear machining method for inner gear. Then [13, 14], a design method of error-free spur slice cutter was obtained; the structure of the rake face was determined according to technological realization of the design, manufacturing, and tool grinding. Although they laid a foundation for the study of spur cutter optimization and tool life, the more complex tapered skiving cutter was not designed and calculated. Stadtfeld [15] presented an optimal opportunity for the skiving process, including the power skiving machine setup definitions, optimization of chip load, high-speed carbide cutter for power skiving, cooling method, and measurement results.

This work aims to investigate the cutting mechanism, including the principle of power skiving, design of tapered skiving cutter, chip formation, and skiving accuracy with respect to the workpiece and cutter parameters.

2 Principle of gear power skiving

Skiving is a continuous chip removal method for universal gear manufacturing. In this manufacturing technology, it is performed different from hobbing and sharping. A tool is placed in a cross-axis angle relative to the workpiece, similar to the shaving process; chip building is initiated by the relative velocity between tool and workpiece. The geometric setup of a skiving cutter relative to an internal gear is shown in Fig. 1. Consider that Cartesian coordinate systems $S_1(O_1\text{-}x_1,y_1,z_1)$ and $S_2(O_2\text{-}x_2,y_2,z_2)$ are rigidly connected to the coordinate of workpiece and skiving cutter, respectively. The front view of the generating gear system is shown in the upper graphic, the internal gear is oriented in the coordinate system S_1 with its axis of rotation collinear to the z_1-axes, and the skiving cutter is oriented in the coordinate system S_2 with its axis of rotation collinear to the z_2-axes. The cutter center is positioned out of the center of xy plane by a radial distance vector a. The pitch circles of the gear and cutter contact tangentially at the lowest point of the pitch circle. The top view, which shows the tool shaft angle Σ between workpiece axes and skiving cutter axes, is drawn below the front view. In case of spur gear, the stroke motion $\boldsymbol{v}_0^{(2)}$ is directed in line with the z_1-axis. The workpiece and cutter perform with an angular velocity ω_1 and ω_2, respectively. When the axial feed motion $\boldsymbol{v}_0^{(2)}$ is increasing, the workpiece rotates about z_1-axes by φ_1 and the cutter rotates about z_2-axes by φ_2.

The cutting velocity $\boldsymbol{v}_c$ results form positioning constraints during the rolling of the generation train and uses the resulting relative movement of workpiece and skiving cutter. Therefore, the cutting velocity depends on the number of revolution of

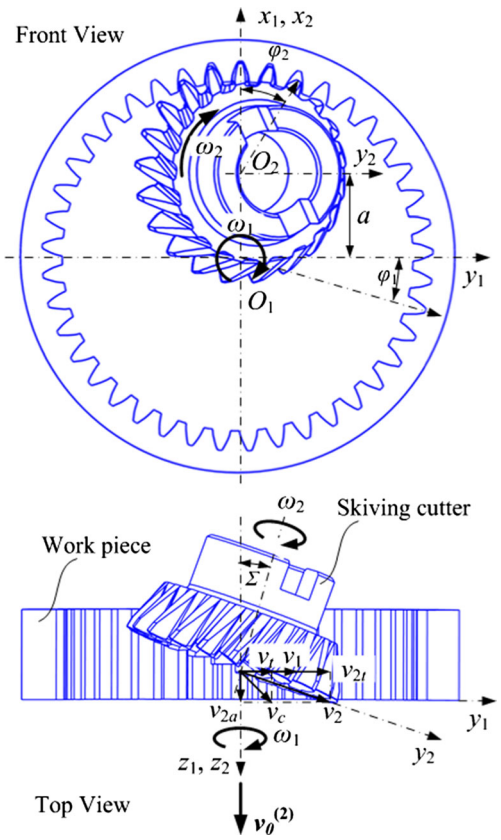

Fig. 1 Kinematical principle of power skiving for an internal cylindrical gear

the generation train and the shaft angle. As shown in Fig. 1, the cutter velocity $\boldsymbol{v}_2$ is divided into the axial speed $\boldsymbol{v}_{2a}$ and tangential velocity $\boldsymbol{v}_{2t}$. Then, the tangential velocity $\boldsymbol{v}_{2t}$ and the workpiece $\boldsymbol{v}_1$ result in the resultant tangential velocity $\boldsymbol{v}_t$. Consequently, the cutting velocity $\boldsymbol{v}_c$ results from the axial speed $\boldsymbol{v}_{2a}$ and the resultant tangential speed $\boldsymbol{v}_t$.

In case of working a helical gear, the stroke motion is oriented in z_1-axis direction, but an incremental angular velocity $\Delta\omega_1$, which depends on the axial feed, has to be added to ω_1. The incremental angular velocity of workpiece, $\Delta\omega_1$, is determined by the following equation:

$$\Delta\omega_1 = \frac{2v_0^{(2)}\sin\beta_1}{m_n Z_g} \tag{1}$$

where $\boldsymbol{v}_0{}^{(2)}$ is the axial stroke feed, m_n is the normal module of tooth, Z_g is the tooth number of workpiece, and Z_t is the tooth number of skiving cutter.

Therefore, the relationship between the angular velocity of workpiece and cutter and axial feed satisfies the following relation:

$$\omega_1 = \frac{Z_t}{Z_g}\omega_2 - \frac{2v_0^{(2)}\sin\beta_1}{m_n Z_g} \tag{2}$$

On the contrary, if the workpiece provides the incremental movement, the relation can be represented as

$$\omega_2 = \frac{Z_g}{Z_t}\omega_1 - \frac{2v_0^{(2)}\sin\beta_1}{m_n Z_t} \tag{3}$$

3 Calculation of skiving cutter profile

3.1 The equation of meshing

Skiving process can be investigated as a pair of helical crossed gear engagement, so the tool profile should satisfy the equation of meshing [16], [17]

$$\begin{aligned} &v^{(12)}\cdot n = 0 \\ &\left(w^{(1)}\times r^{(1)} - w^{(2)}\times r^{(2)} + v_0^{(1)} - v_0^{(2)}\right)\cdot n = 0 \end{aligned} \tag{4}$$

The relative velocity $\boldsymbol{v}^{(12)}$ is expressed as

$$\begin{aligned} \mathbf{v}^{(12)} = {} & (-\omega_1 y - \omega_2 z\sin\Sigma + \omega_2 y\cos\Sigma)\mathbf{i} + [\omega_1 x - \omega_2(x+a)\cos\Sigma - v_{02}\sin\Sigma]\mathbf{j} \\ & + [\omega_2(x+a)\sin\Sigma + v_{01} - v_{02}\cos\Sigma]\mathbf{k} \end{aligned} \tag{5}$$

Consider that the tool surface is represented by the vector equation

$$\mathbf{r}^{(1)} = \mathbf{r}^{(1)}(u,\theta) = x_1(u,\theta)\mathbf{i} + y_1(u,\theta)\mathbf{j} + z_1(u,\theta,p)\mathbf{k} \tag{6}$$

where (u,θ) are the surface parameters; p is the screw parameter in the screw motion about the z_1 axis. The normal to the surface is represented as

$$\begin{aligned} \mathbf{n}^{(1)} = \frac{\partial \mathbf{r}^{(1)}}{\partial u}\times\frac{\partial \mathbf{r}^{(1)}}{\partial \theta} &= \begin{vmatrix} \mathbf{i}_1 & \mathbf{j}_1 & \mathbf{k}_1 \\ \dfrac{\partial x_1}{\partial u} & \dfrac{\partial y_1}{\partial u} & \dfrac{\partial z_1}{\partial u} \\ \dfrac{\partial x_1}{\partial \theta} & \dfrac{\partial y_1}{\partial \theta} & \dfrac{\partial z_1}{\partial \theta} \end{vmatrix} \\ &= n_x^{(1)}\mathbf{i}_1 + n_y^{(1)}\mathbf{j}_1 + n_z^{(1)}\mathbf{k}_1 \end{aligned} \tag{7}$$

Combining the relative velocity in Eq. (5) with the vector equation in Eq. (7) yields the following meshing equation

$$\begin{aligned} & n_x^{(1)}\{(-y - i_{21}\sin\Sigma + i_{21}y\cos\Sigma)\omega_1 + (-i''\sin\Sigma + i''y\cos\Sigma)v_{02}\} + \\ & n_y^{(1)}\{(y - i_{21}(x+a)\cos\Sigma)\omega_1 + [-i_{21}(x+a)\cos\Sigma - \sin\Sigma]v_{02}\} + \\ & n_z^{(1)}\{(i_{21}(x+a)\sin\Sigma)\omega_1 + [i_{21}(x+a)\sin\Sigma - \cos\Sigma]v_{02}\} = 0 \end{aligned} \tag{8}$$

where i_{21} indicates the ratio between workpiece and skiving cutter, $i'' = \frac{2\sin\beta_1}{m_n z_g}$, β_1 is the helical angle of workpiece.

According to the *Principle of Gearing* [15], the angular velocity ω_1 and the axial feed v_{02} are independent with a two-degree-of-freedom engagement movement, thus

$$\begin{cases} n_x^{(1)}(-y - i_{21}\sin\Sigma + i_{21}y\cos\Sigma) + n_y^{(1)}(y - i_{21}(x+a)\cos\Sigma) + n_z^{(1)}(i_{21}(x+a)\sin\Sigma) = 0 \\ n_x^{(1)}(-i''\sin\Sigma + i''y\cos\Sigma) + n_y^{(1)}(-i_{21}(x+a)\cos\Sigma - \sin\Sigma) + n_z^{(1)}(i_{21}(x+a)\sin\Sigma - \cos\Sigma) = 0 \end{cases} \tag{9}$$

After the coordinate transformation, the meshing equation is represented as follows:

$$\begin{cases} U_1\cos\varphi_1 - V_1\sin\varphi_1 = W_1 \\ U_2\cos\varphi_1 - V_2\sin\varphi_1 = W_2 \end{cases} \tag{10}$$

where

$$\begin{cases} U_1 = i_{21}\left(-z_1 n_{x_1}^{(1)}\sin\Sigma - a n_{y_1}^{(1)}\cos\Sigma + x_1 n_{z_1}^{(1)}\sin\Sigma\right) \\ V_1 = i_{21}\left(-z_1 n_{y_1}^{(1)}\sin\Sigma + a n_{x_1}^{(1)}\cos\Sigma + y_1 n_{z_1}^{(1)}\sin\Sigma\right), \\ W_1 = (1-i_{21}\cos\Sigma)\left(y_1 n_{x_1}^{(1)} - x_1 n_{y_1}^{(1)}\right) - a i_{12} n_{z_1}^{(1)}\sin\Sigma \end{cases}$$

$$\begin{cases} U_2 = i''\left(-z_1 n_{x_1}^{(1)}\sin\Sigma - a n_{y_1}^{(1)}\cos\Sigma + x_1 n_{z_1}^{(1)}\sin\Sigma\right) - n_{y_1}^{(1)}\sin\Sigma \\ V_2 = i''\left(-z_1 n_{y_1}^{(1)}\sin\Sigma + a n_{x_1}^{(1)}\cos\Sigma + y_1 n_{z_1}^{(1)}\sin\Sigma\right) + n_{x_1}^{(1)}\sin\Sigma, \\ W_2 = -i''\left(y_1 n_{x_1}^{(1)} - x_1 n_{y_1}^{(1)}\right)\cos\Sigma + \left(\cos\Sigma - a i''\sin\Sigma\right) n_{z_1}^{(1)} \end{cases}$$

When the angle φ_1 is given, there is one solution (u,θ) meets the requirements of Eq. (7). Equations (4), (5), (7), and (7), yield

$$\frac{y_1 n_{x_1}^{(1)} - x_1 n_{y_1}^{(1)}}{i_{21}} - \frac{n_{z_1}^{(1)}\cos\Sigma + n_{y_1}^{(1)}\sin\Sigma\cos\varphi_1 + n_{x_1}^{(1)}\sin\Sigma\sin\varphi_1}{i''} = 0 \tag{11}$$

3.2 Equations of tooth profile

Equations of gear tooth profile in transverse plane is represented as

$$\begin{cases} x_0 = r_b\cos(\sigma_0 + u) + r_b u\sin(\sigma_0 + u) \\ y_0 = r_b\sin(\sigma_0 + u) - r_b u\cos(\sigma_0 + u) \end{cases} \tag{12}$$

where r_b is the radius of base circle; σ_0 is the half of angular tooth thickness on the base circle.

The normal to the transverse tooth profile is

$$\begin{cases} x_0' = r_b\cos(\sigma_0 + u) \\ y_0' = r_b\sin(\sigma_0 + u) \end{cases} \tag{13}$$

Using the coordinate transformation, we obtain the tooth profile by the equations

$$\begin{cases} x_1 = x_0\cos(\theta + \varphi_2) + y_0\sin(\theta + \varphi_2) \\ y_1 = x_0\sin(\theta + \varphi_2) - y_0\cos(\theta + \varphi_2) \\ z_1 = p(\theta + \varphi_2) \end{cases} \tag{14}$$

Similarly, the tooth profile is obtained in the coordinate system of skiving cutter by the following equations:

$$\begin{cases} x_2 = (x_1\cos\varphi_1 - y_1\sin\varphi_1 + a)\cos\varphi_2 \\ \quad + \left[(x_1\sin\varphi_1 + y_1\cos\varphi_1)\cos\Sigma - z_1\sin\Sigma\right)\Big]\sin\varphi_2 \\ y_2 = -(x_1\cos\varphi_1 - y_1\sin\varphi_1 + a)\sin\varphi_2 \\ \quad + \left[(x_1\sin\varphi_1 + y_1\cos\varphi_1)\cos\Sigma - z_1\sin\Sigma\right)\Big]\cos\varphi_2 \\ z_2 = (x_1\sin\varphi_1 + y_1\cos\varphi_1)\sin\Sigma + z_1\cos\Sigma - l_2 \end{cases} \tag{15}$$

where l_2 is the incremental movement of cutter.

3.3 Equations of cutting blade in normal plane

Due to the top rake angle γ_z on the front face of skiving cutter, the cutting blade on the front face can be calculated by

$$(x_2 + r)\tan\gamma_z + y_2\sin\Sigma - z_2\cos\Sigma = 0 \tag{16}$$

where r is the radius of skiving cutter in pitch circle; γ_z is the top rake angle.

Equations (9), (13), and (14) yield the cutter blade

$$\begin{cases} x_2 = (x_1\cos\varphi_1 - y_1\sin\varphi_1 + a)\cos\varphi_2 \\ \quad + \left[(x_1\sin\varphi_1 + y_1\cos\varphi_1)\cos\Sigma - z_1\sin\Sigma\right)\Big]\sin\varphi_2 \\ y_2 = -(x_1\cos\varphi_1 - y_1\sin\varphi_1 + a)\sin\varphi_2 \\ \quad + \left[(x_1\sin\varphi_1 + y_1\cos\varphi_1)\cos\Sigma - z_1\sin\Sigma\right)\Big]\cos\varphi_2 \\ z_2 = (x_1\sin\varphi_1 + y_1\cos\varphi_1)\sin\Sigma + z_1\cos\Sigma - l_2 \\ (x_2 + r)\tan\gamma_z + y_2\sin\beta' - z_2\cos\beta' = 0 \\ \dfrac{y_1 n_{x_1}^{(1)} - x_1 n_{y_1}^{(1)}}{i_{21}} - \dfrac{n_{z_1}^{(1)}\cos\Sigma + n_{y_1}^{(1)}\sin\Sigma\cos\varphi_1 + n_{x_1}^{(1)}\sin\Sigma\sin\varphi_1}{i''} = 0 \end{cases} \tag{17}$$

According to the meshing Eq. (9), x_0', y_0', $n_{x_1}^{(1)}$, $n_{y_1}^{(1)}$, and $n_{z_1}^{(1)}$ are relative to the parameter u, and p, Σ, i'', and i_{21} are constant. Therefore, assume that u is equal to $(\theta+\varphi_1)$; we can solve the parameter u.

$$\theta = n_{z_1}^{(1)}\frac{[x_0\cos(\theta+\varphi_1) - y_0\sin(\theta+\varphi_1)]\sin\Sigma - \left(\dfrac{1}{i_{21}} - \cos\Sigma + \dfrac{a i''\cot\Sigma}{i_{21}}\right)p + \dfrac{a}{\sin\Sigma}}{p^2\left[x_0'\sin(\theta+\varphi_1) + y_0'\cos(\theta+\varphi_1)\right]\sin\Sigma} \tag{18}$$

Then, substituting Eq. (9) into Eq. (7) yields the tooth parameter θ, that is $\theta=\theta(u)$, so the rotation angle φ_1 can be derived by subtracting θ form $(\theta+\varphi_1)$. Consequently, we obtain the cutter blade equations by substituting the parameters u, θ, and φ_1 into Eq. (15).

To facilitate manufacture and measure for cutter profile, the normal cutting blade not only parallel to the front face but perpendicular to the direction of cutter surface should be calculated (Fig. 2). The normal cutter profile in the section of N-N is represented as

$$\begin{cases} x_N = -x_2\cos\gamma_z + y_2\sin\gamma_z\sin\Sigma - z_2\sin\gamma_z\cos\Sigma \\ y_N = y_2\cos\Sigma + z_2\sin\Sigma \end{cases} \quad (19)$$

4 Power skiving process and simulation

4.1 Skiving process simulation

The tapered skiving cutter can be achieved according to the cutter profile in Eq. (17). Fig. 3 presents the cutting blade definitions and graphics in skiving process, f_z is axial feed per gear rotation, a_p is radial feed, h_D is nominal maximum chip thickness, γ_z is top rake angle, α_z is top relief angle, λ_z is side relief angle, Σ is shaft angle, n_1 is cutter rotation, v_t is axis in-feed velocity (Fig. 4).

4.2 Chip deformation

Considering the chip removal capacity and the working efficiency, an in-feed strategy for optimized chip formation is produced with 5 cuts based on an oscillating motion between the leading and trailing flank per cut. The 1st cut depth is 1.75 mm, the 2nd cut depth is 1.5 mm, the 3rd cut depth is 2 mm, the 4th cut depth is 1 mm, and the 5th cut depth is 0.5 mm. Fig. 5 presents the in-feed strategy and chip deformation mechanism with different cuts.

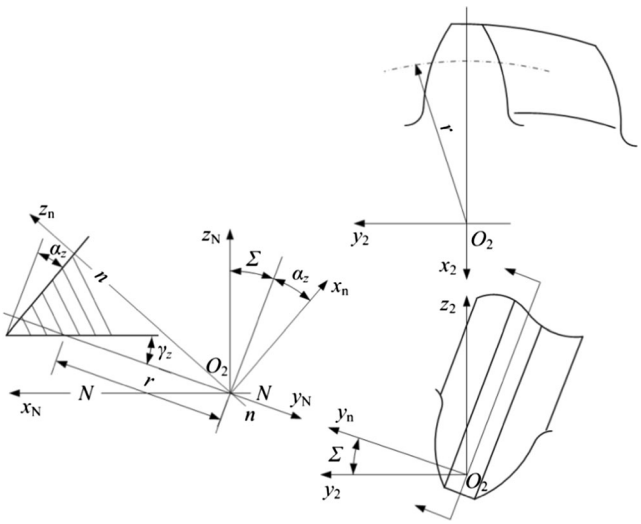

Fig. 2 Calculation of normal cutting blade

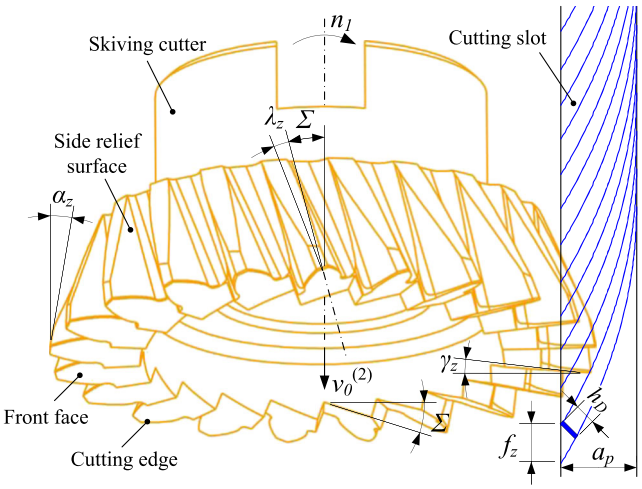

Fig. 3 Cutting blade definitions and graphics

Power skiving chips with a 5× magnification are shown in Fig. 6. The 1st chip is a side I-sharped chip from the 1st cut of a module 3.0 mm gear with a 1.75 mm feed. The 2nd chip is L-shaped from the 2nd cut with a 2 mm feed. The 3rd and 4th chip is U-sharped, which means the side chips and the bottom chip have not been separated. This chip is from the 3rd and 4th cut. The 5th chip is from a finishing cut with a 0.5 mm feed. Fig. 6 shows the chips of different cuts. The upper of the chips are thinner than the lower of chips, and a crack in the middle of the rolled-up sidewall can be observed. The chips deformation indicates that the left channel wall has a more complex shape than the right side (see Fig. 5), and the skiving kinematic provides slightly different cutting conditions on both flanks. The different chip thickness explains the difference of cutting lines above.

The chip deformation from the different cuts shows on the same level of cutter related load to a different sharp of the chips. The shown U-sharp chips are on a high level of collision by themselves, and the chip flow area is very close to the cutting edge, which will increase the cutting forces. By generation, only L-sharp or I-sharp chips, the level of chip flow interference is reduced. The chip flow area on the rake face is larger distance from the cutting edge, and due to that effect, the cutting forces will be decreased.

5 Cutter top rake angle

According to the principle of metal cutting, cutter's rake angle relates to the tool's wear and strength. The more the rake angle is, the more the cutting forces. However, the increasing rake angle will increase the tool's wear. So, a proper rake angle should be taken into

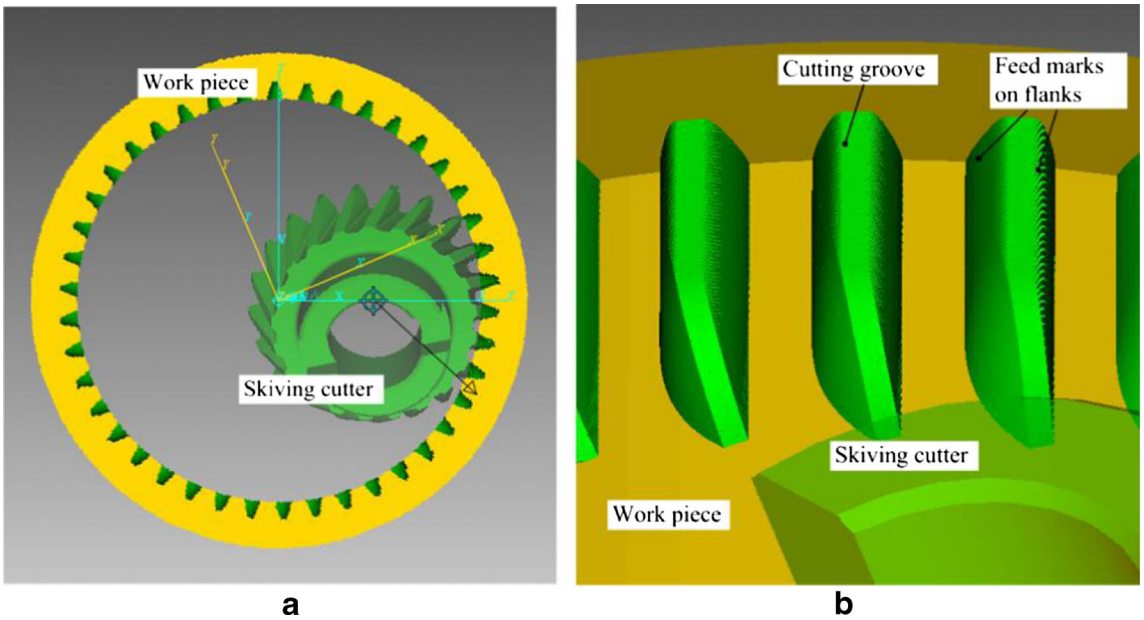

Fig. 4 Skiving process simulation

consideration during the cutting process. The graphic in Fig. 7(a) shows a typical plot of the cutting top rake angle when performing a 5-cut strategy. Since the sweep locus of cutter top is the elliptic equation from the side view of workpiece, see Fig. 7(b), we can obtain the cutter top rake angle in Eq. (18) by the differential geometry relationship.

$$\gamma_z' = a\tan\left(\frac{y'}{x'}\right) - \gamma_z = -a\tan\left(\frac{b}{a}\tan t\right) - \gamma_z \tag{20}$$

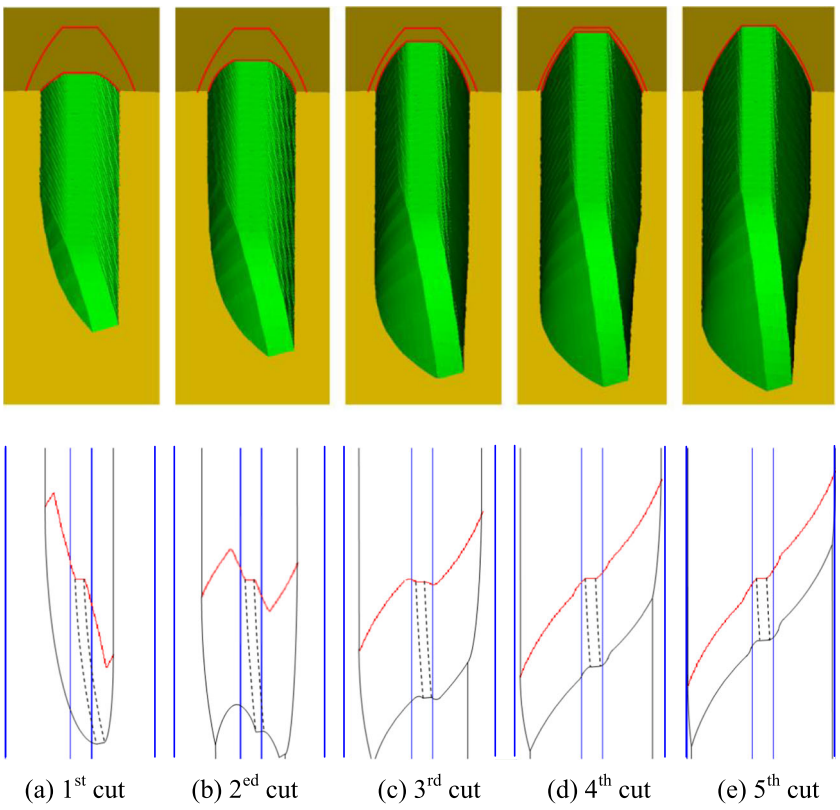

Fig. 5 In-feed strategy and chip deformation mechanism

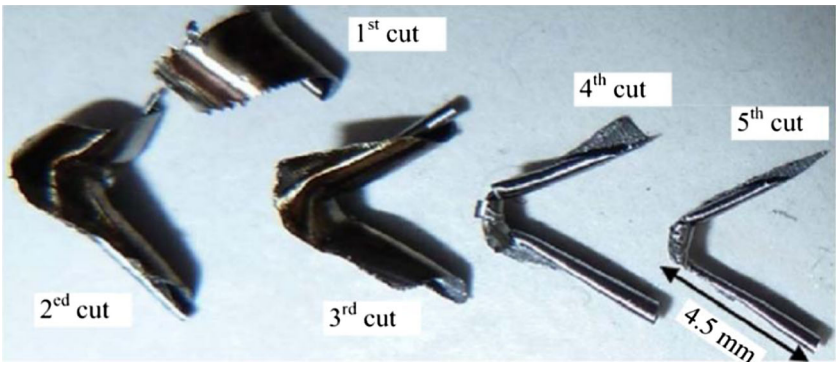

Fig. 6 Chips of different cuts

Where $a = \frac{m_n Z_t}{2\cos\Sigma} - 1.25m_n + \sum_{i=1}^{n} a_p(i)$, $b = a \cdot \sin\Sigma$, $a_p(i)$ is cut depth in cut strategy, $t = a\cos\left(1 - \frac{a_p(i)}{\frac{m_n Z_t}{2\cos\Sigma} - 1.25m_n + \sum_{i=1}^{n} a_p(i)}\right)$.

The top rake angle is determined by the shaft angle and the tooth number of cutter, see Fig. 8. When the shaft angle is increasing, the top rake angle is decreasing. When the cutter tooth number, as well as the diameter of cutter is increasing, it also decreases the top rake angle. At the same time, more cuts induce a decreased top rake angle. Therefore, a better cutting condition with respect to the top rake angle can be obtained by setting a larger shaft angle, choosing a larger cutter diameter, and using more cuts strategy if possible.

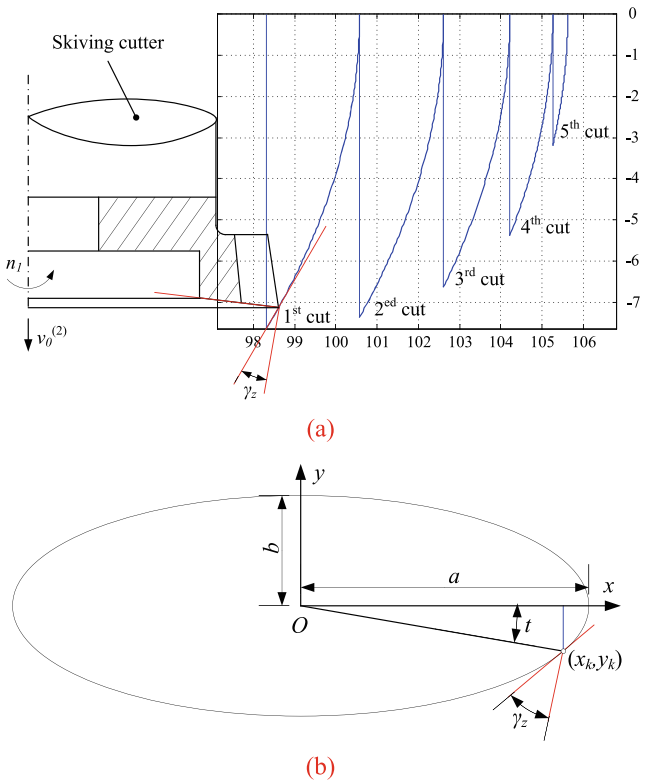

Fig. 7 Calculation of cutter top rake angle

6 Skiving accuracy and cutting parameters

As discussed above, the axial stroke motion with an incremental feed makes the waved feed marks on the flanks. The depth of feed marks, which induce the tooth deviations on the flanks and in root, correlate with the different process parameters such as the tooth ratio between gear and cutter, the axial feed velocity (Table 1). The power skiving accuracy is evaluated and calculated exactly by the proposed mathematical model. However, there are too many figures about lead deviations; the lead deviations related to the cutting parameters are presented in Tables 2 and 3.

6.1 Tooth ratio and processing lead deviations

To investigate the tooth lead deviations related to the gear tooth number, the gear tooth number is divided into the odd number and the even number. Besides, the tooth ratio between gear and cutter is considered. Table 2 and Fig. 9 present the lead deviations related to the tooth number and tooth ratio. When the cutter feed per gear rotation f_z=0.3 mm/r, for odd number of tooth Z_g=63, very small feed marks (F_β=1.3 μm) are possible for gears which have odd number of tooth when a cutter (Z_t=42) with 2/3, the gear tooth number is used. The tooth ratio can be expressed as Z_g*(2/3)=Z_t, the greatest common divisor Z_{GCD}=21, that means every third rotation of the cutter cuts the same gap every second gear rotation. For even number of tooth Z_g=64, very small feed marks (F_β=0.2 μm) are possible for gears which have even number of tooth when a cutter (Z_t=32) with half the gear tooth number is used. The tooth ratio can be expressed as Z_g*(1/2)=Z_t, the greatest common divisor Z_{GCD}=32, that means every second rotation of the cutter cuts the same gap every gear rotation.

Besides, if the tooth ratio is about half number of gear except for the gear number is even and the tooth ratio is

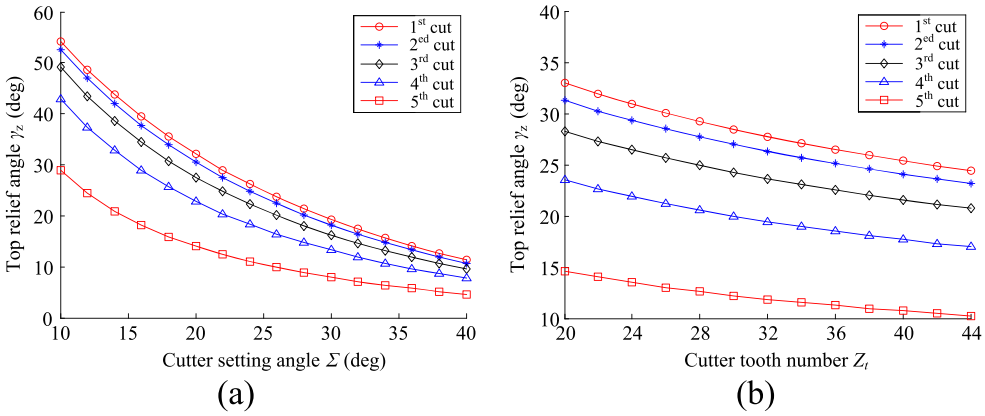

Fig. 8 Top rake angle related to cutter setting angle and cutter tooth number

exactly the half number of gear, then the lead deviations are larger than others. For the odd number of tooth Z_g=63, see Fig. 9a, when the cutter number is 30, 31, 32, and 33, the lead deviations up to the most (F_β=20.2 μm). For the even number of tooth Z_g=64, see Fig. 9b, when the cutter number is 31 and 33 (except 32), the lead deviations up to the most (F_β= 20.2 μm).

Since the tooth ratio between gear and cutter determines the lead deviations on the flanks, the tooth accuracy can be improved by selecting the suitable cutter tooth number. For one thing, regarding high workpiece flanks quality, the cutter number should be divided with the greatest common divisor. For another thing, it is required to avoid using a cutter with half the gear tooth number except that the gear number is even and the tooth ratio is exactly the half number of gear.

Table 1 Basic parameters for power skiving process in the numerical example

Items	Units	
(I) Workpiece data (spur gear)		
Tooth number Z_g	63	–
Module m_n	3	mm
Pressure angle α_n	20	deg
Addendum circle d_a	183	mm
Dedendum circle d_f	196.5	mm
Gear width b	50	mm
(II) Cutter data (tapered cutter)		
Tooth number of cutter Z_t	21	–
Module m_n	3	mm
Helix angle β_2	20	deg
Top rake angle γ_z	5	deg
Top relief angle α_z	12	deg
Side relief angle λ_z	4.5	deg
Outside diameter d_2	74.723	mm
(III) Machine setting data		
Shaft angle Σ	20	deg
Setting distance a	26.957	mm
Rotation of gear n_1	1000	r/min
Rotation of cutter n_2	1500	r/min
Chip thickness ε	0.25	mm
Axial feed of cutter f_z	0.3	mm/r
Processing time t	2.5	min

6.2 Axial feed and processing lead deviations

Reducing the axial feed per gear revolution can further reduce the depth of feed marks. The lead deviations related to the axial feed of cutter are given in Table 3 and

Table 2 Lead deviations related to the tooth number and tooth ratio/μm

	Odd number Z_g=63, f_z=0.3 mm/r		Even number Z_g=64, f_z=0.3 mm/r	
Z_t	F_β in root	F_β on flanks	F_β in root	F_β on flanks
42	1.3	0.4	7.3	2.4
41	6.1	2.0	6.6	2.2
40	7.5	2.5	3.8	2.4
39	5.9	1.9	5.7	1.8
38	6.3	2.1	5.7	1.8
37	7.2	2.4	5.9	1.9
36	5.9	1.9	7.5	2.5
35	7.8	2.6	10.7	3.5
34	13.0	4.3	16.6	5.4
33	19.7	6.5	20.2	6.7
32	20.2	6.7	0.2	0.13
31	20.2	6.7	20.1	6.7
30	18.5	6.2	15.5	5.1
29	11.9	3.9	9.9	3.3
28	7.5	2.5	7.3	2.4
27	3.5	2.5	6.6	2.2
26	7.8	2.6	6.1	2.0

Table 3 Lead deviations related to the axial feed of cutter/um

	Z_g=63, Z_t=36		Z_g=64, Z_t=32	
f_z	F_β in root	F_β on flanks	F_β in root	F_β on flanks
0.1	0.7	0.2	0.08	0.03
0.2	2.6	0.9	0.12	0.09
0.3	5.9	1.9	0.2	0.13
0.4	10.4	3.4	0.35	0.21
0.5	14.1	4.7	0.7	0.4
0.6	15.9	5.3	1.1	0.53
0.7	18.0	6.0	1.7	0.7
0.8	20.0	6.7	2.3	0.9
0.9	20.2	6.7	2.9	1.2
1.0	20.4	6.8	3.1	1.4

Fig. 10. As the amount of axial feed is increasing, the lead deviations are increasing. For example, when f_z=0.5 mm/r and Z_g=63, Z_t=36, the tooth lead deviation F_β=14.1 μm. However, when f_z=0.5 mm/r and Z_g=64, Z_t=32, the tooth lead deviation F_β=0.7 μm. Hence, the feed marks on flanks are relative to the axial feed and the tooth ratio. For the number of gear and cutter with the greatest common divisor, the processing efficiency should be taken into consideration by selecting a larger axial feed. If the number of gear does not match an existing cutter number, then the axial feed has to be chosen until the lead deviations meet the processing requirement. However, if the axial feed is so little that it is also against the cutting process, not only the cycle time is increased but also a tiny chip increases the level of chip flow interference.

7 Conclusions

This paper has established a kinematic model for the latest power skiving technology. Based on the principle of power skiving and mathematical model of tapered skiving cutter, we investigated the cutting mechanism, including the process simulation, chip deformation, cutter rake angle, and skiving accuracy with respect to the gear and cutter parameters. The performed investigation allows to make the following conclusions:

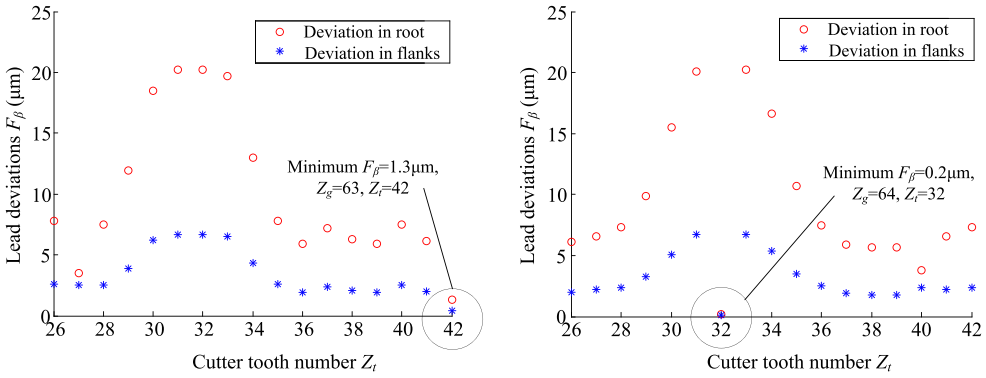

Fig. 9 Lead deviations related to the tooth number and tooth ratio

(a) Odd number of gear tooth (Z_g=63) (b) Even number of gear tooth (Z_g=64)

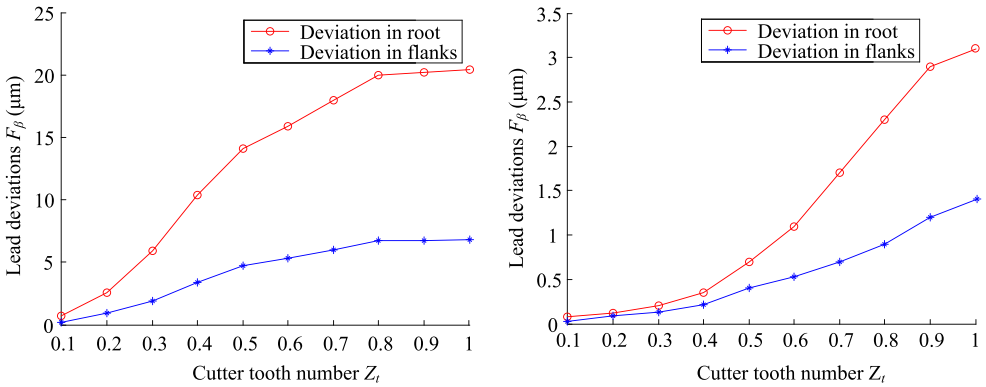

Fig. 10 Lead deviations related to the axial feed of cutter

(a) Odd number of gear tooth (Z_g=63) (b) Even number of gear tooth (Z_g=64)

(1) The chip deformation from the different cuts shows the cutter load to a different sharp of the chips. U-sharp chips are on a high level of collision by themselves and may increase the cutting forces. L-sharp or I-sharp chips can reduce the level of chip flow interference.
(2) When the shaft angle and the cutter diameter is increasing, the top rake angle is decreasing. A better cutting condition with respect to the top rake angle can be obtained by setting a larger shaft angle, choosing a larger cutter diameter and using more cuts strategy if possible.
(3) The tooth ratio between gear and cutter determines the lead deviations on the flanks. Regarding high flanks quality, the cutter number should be divided with a greatest common divisor, and it is required to avoid using a cutter with half the gear tooth number except that the gear number is even and the tooth ratio is exactly the half number of gear.
(4) Reducing the axial feed of cutter can further reduce the depth of feed marks. For the number of gear and cutter with the greatest common divisor, the processing efficiency should be taken into consideration by selecting a larger axial feed. If the number of gear does not match an existing cutter number, the axial feed has to be chosen until the lead deviations meet the processing requirement.

Acknowledgments The authors are grateful to the National Natural Science Foundation of China (No. 51175242) and the financial support of the China Ministry of Science and Technology Innovation Fund for Technology Enterprise (No. 13C26213202060).

References

1. Kojima M (1974) Gear skiving of involute internal spur gear (part 1: on the tooth profile). Bull JSME 17(106):511–518
2. Kojima M (1974) On the clearance angles of skiving cutter (part 2: helical type cutter for internal spur gear skiving). Bulle JSME 17(105):401–408
3. Kobialka C (2012) Contemporary gear pro-machining solutions. AGMA Tech Pap, 12FTM11
4. Lao QC, Liu B (2014) Summary of skiving. Tool Eng 48(1):7–9
5. Spath D, Huhsam A (2002) Skiving for high-performance machining of periodic structures. Ann CIRP 51(1)
6. Fleischer J, Bechle A, Kuhlewein C (2006) Process development of skiving-a highly productive gearing process. CIRP January Meeting, Presentation STC-C, Paris
7. Fleischer J, Bechle A, Kuhlewein C (2006) High performance gearing by skiving. CIRP 2nd International Conference on High Performance Cutting (HPC), Canada
8. Volker S, Chirsttoph K, Hermann A (2011) 3D-FEM modeling of gear skiving to investigate and chip formation mechanisms. Adv Mater Res 223:46–55
9. Hartmut M, Olaf V (2012) Robust method for skiving and corresponding apparatus comprising a skiving tool. US patent, 20120328384A1
10. Hartmut M, Olaf V (2013) Semi-completing skiving method and device having corresponding skiving tool for executing a semi-completing skiving method. US patent, 20130071197A1
11. Li J, Chen XC, Zhang HY (2011) Slicing technology for cylindrical gears. Chin J Mech Eng-En 47(19):193–198
12. Chen XC, Li J, Lou BC (2013) A study on the design of error-free spur slice cutter. Int J Adv Manuf Technol 68(4): 727–738
13. Chen XC, Li J, Lou BC (2013) Effect of the cutter parameters and machining parameters on the interference in gear slicing. Chin J Mech Eng-En 26(6):1118–1126
14. Chen XC, Li J, Peng W (2014) A study on the grinding of the major flank face of error-free spur slice cutter. Int J Adv Manuf Technol 72(2):425–438
15. Stadtfeld H (2014) Power skiving of cylindrical gears on different machine platforms. Gear Technol 1:52–62
16. Wu XT (2009) Principle of gearing (2th ed). Xi'an Jiaotong University Press, China
17. Litvin FL, Fuentes A (2004) Gear geometry and applied theory (2nd ed). Cambridge University Press, New York